

Tricritical point with fractional supersymmetry from a Fibonacci topological state

Wen-Tao Xu¹ and Guang-Ming Zhang^{1,2}

¹State Key Laboratory of Low-Dimensional Quantum Physics and
Department of Physics, Tsinghua University, Beijing 100084, China

²Collaborative Innovation Center of Quantum Matter, Beijing 100084, China.

(Dated: May 27, 2019)

We consider a generic Fibonacci topological wave function on a square lattice, and the norm of this wave function can be mapped into the partition function of two-coupled ϕ^2 -state Potts models with $\phi = (\sqrt{5} + 1)/2$ as the golden ratio. A global phase diagram is thus established to display non-abelian topological phase transitions. The Fibonacci topological phase corresponds to an emergent new phase of the two-coupled Potts models, and continuously change into two non-topological phases separately, which are dual each other and divided by a first-order phase transition line. Under the self-duality, the Fibonacci topological state enters into the first-order transition state at a quantum tricritical point, where two continuous quantum phase transitions bifurcate. All the topological phase transitions are driven by condensation of anyonic bosons consisting of Fibonacci anyon and its conjugate. However, a fractional supersymmetry is displayed at the quantum tricritical point, characterized by a coset conformal field theory.

Introduction. - In recent years theoretical and experimental search for topological quantum phases of matter with fractionalized anyonic excitations has attracted considerable attention, because non-abelian quasiparticles are necessary ingredient for topological quantum computation [1–3]. The Fibonacci anyons are the simplest example for universal quantum computation. The Fibonacci topological phase contains two types of excitations: the trivial one 1 and non-abelian anyon τ with quantum dimension $d_\tau = \phi$, where $\phi = (\sqrt{5} + 1)/2$ is the golden ratio. They satisfy the non-abelian fusion rule:

$$1 \otimes \tau = \tau \otimes 1 = \tau, \quad \tau \otimes \tau = 1 \oplus \tau. \quad (1)$$

The doubled Fibonacci (DFib) phase has two additional anyons: $\bar{\tau}$ with the opposite chirality to τ and anyon $b = \tau \otimes \bar{\tau}$ as a composite boson. A microscopic lattice model for the DFib topological phase is given by the Levin-Wen string-net model[4]

Since these non-abelian topological phases cannot be described by any local order parameters, the corresponding phase transitions to their adjacent non-topological phases are beyond the conventional Landau-Ginzburg-Wilson paradigm. Previous investigations are devoted to the perturbed Levin-Wen string-net with a competing interaction[5, 6], the wave function deformed by a string tension[7], and a reduced one-dimensional models[8–10]. However, because these models are mostly defined on the trivalent lattice, quantum self-duality as the important feature of the generic doubled topological phases[11, 12] is lacking, i.e., the invariance of interchanging the vertices and plaquettes in the microscopic lattice models. So a generic phase diagram of the DFib topological state has not been established yet.

To incorporate the quantum self-duality into the DFib topological phase, P. Fendley proposed a quantum net wave function[11, 13]. On a square lattice, the corresponding parent Hamiltonian involving simpler interactions than the string-net model. In this Letter, based

on this quantum net wave function, we propose a generic DFib topological wave function with two deformed parameters, and fully develop a wave function approach to the non-abelian topological phase transitions. The norm of this wave function can be mapped into the partition function of two-coupled ϕ^2 -state Potts models, and a generic phase diagram is established. The DFib topological phase represents an emergent new phase of the two-coupled Potts models, while two non-topological phases correspond to the low- and high-temperature phases of the coupled Potts model, respectively, which are dual each other and separated by a first-order transition line. Along the quantum self-duality path, a quantum tricritical point exists between the DFib topological phase and the first-order transition state. Away from the self-duality, we perform the numerical calculations to determine the phase boundaries via the transfer operator of the tensor network method[14]. The corresponding conformal field theories (CFT) of the quantum criticality are fully discussed.

DFib wave function. - On a square lattice, a quantum net wave function is given by[11, 13],

$$|\Psi\rangle = \sum_{\mathcal{N}} \phi^{-L_{\mathcal{N}}/2} \chi_{\mathcal{N}}(\phi^2) |\mathcal{N}\rangle, \quad (2)$$

which is the superposition of nets \mathcal{N} . An edge of the lattice is either empty or occupied by τ string, yielding two orthogonal quantum states labelled by $|1\rangle$ and $|\tau\rangle$, see Fig.1(a). A net is formed by closed τ strings which are allowed to branch and cross, as shown in Fig.1 (b). The superposition weights are given by both chromatic polynomial $\chi_{\mathcal{N}}(Q)$ and a string tension $\phi^{-L_{\mathcal{N}}/2}$, where $L_{\mathcal{N}}$ is the total length of the τ strings in the net \mathcal{N} . The chromatic polynomial $\chi_{\mathcal{N}}(Q)$ can be understood by treating the strings τ in the net \mathcal{N} as the boundaries separating different regions. The dual net $\hat{\mathcal{N}}$ corresponds to a vertex for each region and an edge connecting each pair of regions sharing a boundary. For an integer Q ,

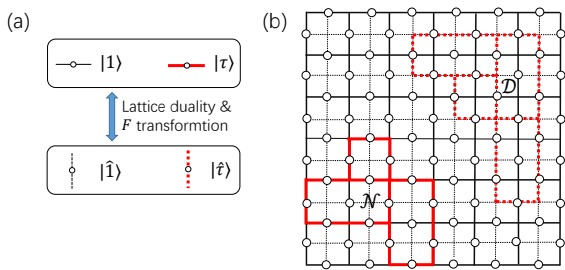


FIG. 1: (a) Two local orthogonal quantum states $|1\rangle$ and $|\tau\rangle$ on an edge of the original lattice, and the transformed states $|\hat{1}\rangle$ and $|\hat{\tau}\rangle$ after the quantum duality. (b) The physical degrees of freedom (open circle) locate at the edges of a square lattice. The full lines are original lattice while the dash lines are dual lattice. \mathcal{N} is a typical net on the original lattice and \mathcal{D} is a net on the dual lattice.

$\chi_{\mathcal{N}}(Q)$ is the number of ways of coloring each region with Q colors such that the neighboring regions are colored differently. Since $\chi_{\mathcal{N}}(Q)$ is a polynomial of Q , we can generalize Q to any non-integers, and the present case $Q = \phi$.

The quantum self-duality of $|\Psi\rangle$ is displayed by rewriting on the dual lattice in a specified representation, whose basis are orthogonal quantum states $|\hat{1}\rangle$ and $|\hat{\tau}\rangle$ on an edge of the dual lattice. As shown in Fig.1 (a), they are related to the local states $|1\rangle$ and $|\tau\rangle$ of the original lattice through the transformation:

$$F = \frac{1}{\phi} \begin{pmatrix} 1 & \sqrt{\phi} \\ \sqrt{\phi} & -1 \end{pmatrix}. \quad (3)$$

After the duality transformation, the wave function $|\Psi\rangle$ in Eq. (25) becomes

$$|\hat{\Psi}\rangle \propto \sum_{\mathcal{D}} \phi^{-L_{\mathcal{D}}/2} \chi_{\mathcal{D}}(\phi^2) |\mathcal{D}\rangle, \quad (4)$$

where \mathcal{D} is the net formed by $\hat{\tau}$ strings on dual lattice, as displayed in Fig. 1 (b). The $|\hat{\Psi}\rangle$ has the same form with $|\Psi\rangle$, thus $|\Psi\rangle$ possess the quantum self-duality[11, 13].

Deformed DFib wave function. - To consider the topological phase transitions out of the DFib phase, we propose a deformed quantum net wave function. Analogous to the self-dual toric code model[12, 15], the deformed wave function is introduced by using spin polarized filters in two dual spin directions:

$$|\Psi(h, \hat{h})\rangle = \prod_{\text{edges}} P_{\text{edge}}(h, \hat{h}) |\Psi\rangle, \quad (5)$$

where $P_{\text{edge}}(h, \hat{h}) = 1 + h\sigma^z + \hat{h}\hat{\sigma}^z$ is the deformation matrix, h and \hat{h} denote the filter strengths in two spin directions. σ^z is the diagonal Pauli matrix in the $|1\rangle$ and $|\tau\rangle$ basis. And $\hat{\sigma}^z = F\sigma^z F^{-1}$, which is diagonal Pauli matrix in the $|\hat{1}\rangle$ and $|\hat{\tau}\rangle$ basis. It is obvious that the quantum duality transforms $|\Psi(h, \hat{h})\rangle$ into $|\Psi(\hat{h}, h)\rangle$, displaying the quantum self-duality when $h = \hat{h}$.

The squared wave function weights can be interpreted as the Boltzmann weights, providing a plasma analogy between topological ground states and the statistical model. So the equal-time correlators of local quantum operators can be mapped to the correlators of different local operators of statistical mechanics model. And the quantum phase transitions are captured by the phase transitions in the statistical model. In the net basis, the norm of the deformed wave function is expressed as

$$\mathcal{Z} = \sum_{\mathcal{N}, \mathcal{N}'} \chi_{\mathcal{N}}(\phi^2) \chi_{\mathcal{N}'}(\phi^2) \prod_{\text{edge}} W_{n_e, n'_e}, \quad (6)$$

where \mathcal{N} and \mathcal{N}' denote the nets in the bra and ket layers, and $n_e = 1$ or τ when the edge e of the net \mathcal{N} is empty or occupied by the τ string. While the chromatic polynomials determine the non-local part of the Boltzmann weights, the local part is given by the matrix

$$W = \begin{pmatrix} Q_{11} & Q_{1\tau}/\sqrt{\phi} \\ Q_{\tau 1}/\sqrt{\phi} & Q_{\tau\tau}/\phi \end{pmatrix}, \quad (7)$$

where Q_{11} , $Q_{1\tau}$, $Q_{\tau 1}$ and $Q_{\tau\tau}$ are elements of the matrix P^2 . It is known that the partition function of a ferromagnetic Q -state Potts model can be expanded as $\mathcal{Z}_{\text{Potts}}(K, Q) = \sum_{\mathcal{N}} e^{-KL_{\mathcal{N}}} \chi_{\mathcal{N}}(Q)$ with the temperature $1/K$. So the partition function (6) describes two-coupled ferromagnetic ϕ^2 -state Potts models, where the local Boltzmann weight matrix W includes the terms $e^{-KL_{\mathcal{N}}}$ and $e^{-KL_{\mathcal{N}'}}$ for each ϕ^2 -state Potts model and coupling between two Potts models.

In the parameter space of (h, \hat{h}) , two special lines can be found from the local Boltzmann weight matrix. When the coupling between two Potts models vanishes, we have two decoupled ϕ^2 -state Potts models, and the local part of Boltzmann weight W_{n_e, n'_e} becomes a product of two local Boltzmann weights of the ϕ^2 -state Potts model,

$$W \propto \begin{pmatrix} 1 & e^{-K} \\ e^{-K} & e^{-2K} \end{pmatrix}. \quad (8)$$

Such a condition is equal to $\det P = 0$, from which an ellipse equation is derived

$$h^2 - 2(2\phi - 3)h\hat{h} + \hat{h}^2 = 1, \quad (9)$$

determining the outer boundary of the phase diagram of the coupled Potts model. According to the above equation, the critical point D of each ϕ^2 -state Potts model can be determined to $h = \hat{h} = \phi/2 \simeq 0.809$. In contrast, as the coupling between two ϕ^2 -state Potts models is strong enough, the coupled model becomes a single ϕ^4 -state Potts model with the local Boltzmann weight

$$W \propto \begin{pmatrix} 1 & e^{-K} \\ e^{-K} & e^{-K} \end{pmatrix}, \quad (10)$$

and another ellipse curve equation can be deduced

$$(h-1)^2 + (\hat{h}-1)^2 - 2h\hat{h}\frac{\phi-1}{\phi+1} = 1. \quad (11)$$

Due to $\phi^4 > 4$, this ϕ^4 -state Potts model can only have a first-order phase transition between the low- and high-temperature gapped phases[16], and the phase transition point S is also determined to $h = \hat{h} = \frac{\phi}{2}(\phi - \sqrt{\phi}) \simeq 0.280$.

More interestingly, along the self-dual line, a new critical point C can be found at $h = \hat{h} \simeq 0.197$ by considering the level-rank duality and the $SO(4)_3$ Birman-Murakami-Wenzl algebra for the transfer matrix of the coupled Potts model in the loop representation[17]. So this quantum critical point divides the self-dual line into two parts: the gapped state ($0 \leq h < 0.197$) corresponding to the DFib topological state and another state ($0.197 < h < 0.809$) corresponding to the non-topological state. Both the perturbed analysis[18] and the first-order nature of the ϕ^4 -state Potts model suggest that the non-topological phase has a small gap. In fact, the ending points of this line ($0.197 < h < 0.809$) are two distinct critical points, and the non-topological gapped state represents a first-order phase transition line.

Global phase diagram. - To establish the global phase diagram, we have to perform numerical calculations with the deformed DFib wave function. For simplicity, we will focus on the parameter regime: $h, \hat{h} \geq 0$. By introducing auxiliary degrees of freedom, the non-local chromatic polynomials are decomposed into a local structure, yielding a triplet-line tensor network state. Starting from the local tensor $T_{\alpha\beta\gamma}^{ijk}$ for the DFib string-net wave function[19, 20], we first define the local tensor $\tilde{T}_{\alpha\beta\gamma}^{ijk} = \phi^{-\frac{3}{4}} \delta_{ij} \delta_{jk} \delta_{k\tau} T_{\alpha\beta\gamma}^{ijk}$. Then, as shown in Fig. 2, the local tensor T_{sq} of the quantum net on the square lattice can be obtained by contracting two triple-line tensors \tilde{T} along one bond direction of the honeycomb lattice. The detailed derivation is included in Supplementary Material. Since the deformation operator P acts on the on-site degrees of freedom, the deformed local tensor $T_{sq}(h, \hat{h})$ is obtained by simply acting \sqrt{P} on the physical indices. The deformed wave function in the tensor network representation is obtained by contracting all virtual indices α, β, γ and θ of the local tensors

$$|\Psi(h, \hat{h})\rangle = \sum_{\{ij\cdots\}} \text{tTr} \left[\bigotimes_{\text{vertex}} \phi^{-\frac{i+j+l+m}{4}} T_{sq}(h, \hat{h}) \right] |ij\cdots\rangle. \quad (12)$$

where "tTr" denotes the tensor contraction and $\phi^{-(i+j+l+m)/4}$ comes from the string tension of the quantum net $|\Psi\rangle$.

Due to lack of local order parameters in the non-abelian topological phase transitions, we have to determine the phase boundaries by employing the quantum fidelity[21] in the numerical calculation with the tensor network wave function. The diagonal elements of the

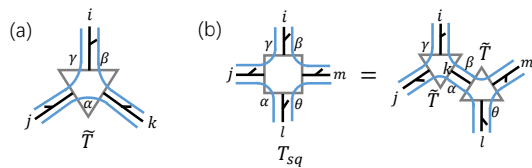


FIG. 2: (a) The triplet-line local tensor $\tilde{T}_{\alpha\beta\gamma}^{ijk}$ of the tensor network state for the string-net model. The legs of the tensor connected by lines (labelled by only one index for simplicity) are locked by the delta function, and the legs pointed outside of the paper are physical indices. (b) Contracting two tensors \tilde{T} along one bond direction of the honeycomb lattice yields the tensor T_{sq} for the quantum net wave function on a square lattice.

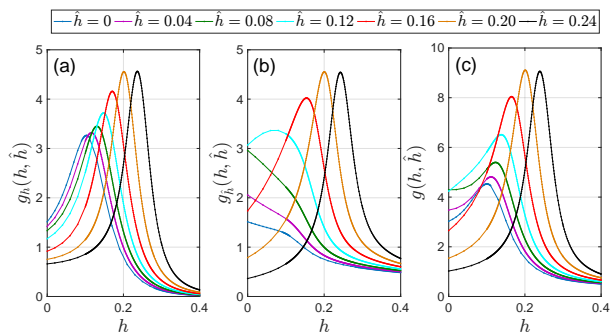


FIG. 3: The fidelity metric calculated from the wave functions with $N = L_y L_x = 4 \times 10$ sites and $\delta h = \delta \hat{h} = 0.005$, where \hat{h} is fixed and h is varied. (a) One diagonal element $g_h(h, \hat{h})$. (b) The other diagonal element $g_{\hat{h}}(h, \hat{h})$. (c) The trace of the fidelity metric $g(h, \hat{h}) = g_h(h, \hat{h}) + g_{\hat{h}}(h, \hat{h})$.

quantum fidelity metric are expressed as

$$g_h(h, \hat{h}) = -\frac{1}{(\delta h)^2 N} \log |\langle \Psi(h, \hat{h}) | \Psi(h + \delta h, \hat{h}) \rangle|,$$

$$g_{\hat{h}}(h, \hat{h}) = -\frac{1}{(\delta \hat{h})^2 N} \log |\langle \Psi(h, \hat{h}) | \Psi(h, \hat{h} + \delta \hat{h}) \rangle|,$$

where N is the total number of lattice sites and $\delta h = \delta \hat{h} = 5 \times 10^{-3}$ is chosen in the calculations. Note that all wave functions in the above expressions are normalized. The quantum duality implies $g_h(h, \hat{h}) = g_{\hat{h}}(\hat{h}, h)$. In Fig.3, for a given value of \hat{h} but different h , we show the diagonal elements of the fidelity metric and its trace value $g_h(h, \hat{h}) + g_{\hat{h}}(h, \hat{h})$, where the peak positions of the curves correspond to the quantum phase transition points[15].

Combining the known analytical results on the self-dual line and numerical results via the quantum fidelity calculations away from the self-duality, we can establish a global phase diagram, as shown in the Fig. 4. Two non-topological gapped phases corresponding to the low-temperature and high-temperature phases of the Potts model are separated by a first-order phase transition line CD . However, the DFib topological phase enclosed by two topological phase transition lines AC and BC repre-

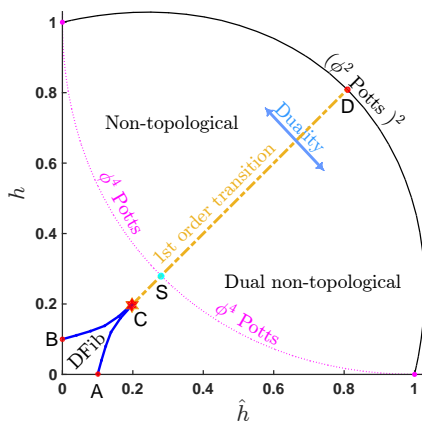


FIG. 4: The global phase diagram of a generic DFib topological phase. The second-order phase transition lines AC and BC are determined by the trace of quantum fidelity metric. Two non-topological phases correspond to the low- and high-temperature phases of the coupled Potts models, while the DFib topological phase is an emergent phase of the coupled Potts model. The point S exactly sits on the first-order transition line, and the point C is the tricritical point. The point D is the critical point of two decoupled ϕ^2 -state Potts models, and each has a central charge $c = 7/10$

sents a new phase of the two-coupled Potts model. Along the self-dual line, the first-order transition line terminates at the critical point D . More importantly, the first-order transition line bifurcates at the quantum critical point C into two separate topological phase transition lines BC and AC . So this quantum critical point C is a quantum tricritical point in the phase diagram. The points A and B on the axes are numerically determined to $(\hat{h} \simeq 0.099, h = 0)$ and $(\hat{h} = 0, h \simeq 0.099)$.

Quantum Criticality. - Along the h axis, the deformation matrix P is diagonal, the phase transition is equivalent to the DFib topological phase transition driven by tuning a string tension. The string-net wave function deformed by a string tension, whose norm is exactly mapped to the $(\phi+2)$ -state Potts model[11, 22], has been studied[7]. However, due to the difference between the quantum net wave function $|\Psi\rangle$ on the square lattice and the string-net one on the honeycomb lattice, the wave function norm of the quantum net can not be exactly mapped to the partition function of the $(\phi+2)$ -state Potts model. Nevertheless, it is argued that the difference is an irrelevant perturbation[11] so that the phase transition of the quantum net wave function still belongs to the same universality class[23]. Actually our numerical calculations confirm this conclusion (see Supplementary Material). So the corresponding critical point is described by the seventh unitary minimal CFT with the central charge $c = 14/15$. This continuous phase transition is driven by the condensation of b anyons consisting of the Fibonacci anyon and its conjugate[7].

Since the quantum critical point B is a conformal quan-

TABLE I: Scaling dimensions $\mathfrak{h}_{p,q} + \bar{\mathfrak{h}}_{p,q}$ of the primary fields in the coset CFT for the quantum tricritical point. The third column gives the numerical values extracted from the transfer operator with a circumference $L_y = 6$, whose eigenvalue spectrum is rescaled such that the scaling dimension of the first descendant for the lowest primary field is unity. The fourth column lists the quantum numbers of the matrix product operator. The data with the absolute errors larger than 10% are indicated by stars, and the last three primary fields have some difficulties to be determined.

(p, q)	$\mathfrak{h}_{p,q} + \bar{\mathfrak{h}}_{p,q}$	Numerical result	quantum number	Absolute error
(1, 1)	0	0	ϕ^2	0
(2, 3)	1/10	0.10692317	-1	0.0069
(1, 2)	9/80	0.11235947	ϕ^{-2}	0.0253
(2, 2)	9/80	0.11235947	ϕ^{-2}	0.0253
(2, 4)	13/80	0.16501496	-1	0.0025
(1, 3)	3/10	0.30662991	-1	0.0066
(2, 5)	3/10	0.30662991	-1	0.0066
(1, 4)	9/16	0.55837990	ϕ^{-2}	0.0041
(3, 7)	3/5	0.67849389	ϕ^{-2}	0.0785
(2, 6)	73/80	0.74175242*	ϕ^2	0.1707
(1, 5)	13/10	0.97123493*	-1	0.3288
(2, 7)	8/5	-	-	-
(1, 6)	169/80	-	-	-
(1, 7)	3	-	-	-

tum critical point[24], all equal-time correlation functions are described by the two dimensional CFT. From the quantum duality, the quantum critical point A on the dual axis \hat{h} has the same property. The validity of the universality hypothesis allows us to further argue that the topological phase transitions across both the AC and BC lines are effectively characterized by the same critical field theory as the $(\phi+2)$ -state Potts model, as there is no other mechanism for the topological quantum phase transition. We notice that a similar situation occurs in the topological phase transitions of the deformed toric-code wave function with duality[12].

Moreover, it is known that the level-rank duality of the coupled Potts model in the loop representation not only determines the position of a tricritical point but also gives rise to the underlying critical field theory[17]. Namely it is the coset CFT[25] of $\frac{SU(2)_3 \times SU(2)_3}{SU(2)_6}$ with a central charge $c = 27/20$, which is regarded as the sum of a bosonic field with a given background screening charge located at infinity and a \mathbb{Z}_3 parafermionic field[26, 27]. This quantum tricritical point C is also a conformal quantum tricritical point, and the scaling dimensions of the primary fields together with our numerical results are listed in Tab.I.

Surprisingly, there emerges a fractional superconformal symmetry at the quantum tricritical point C . Generally, the coset CFT of $\frac{SU(2)_M \times SU(2)_N}{SU(2)_{N+M}}$ is minimal with

respect to the Virasoro algebra extended by a conserved current of extra-symmetry[26, 27]. $N = 1$ gives rise to the series of unitary minimal models, while $N = 2$ yields the series of the unitary minimal superconformal models, where the Virasoro algebra is extended to the super-Virasoro algebra by a conserved current with spin-3/2. This series of models has a superconformal symmetry, including the critical point D ($M = 1$). For $N = 3$, the Virasoro algebra is further extended by a non-local conserved current with spin-7/5, and this series of models has a fractional superconformal symmetry[28–30], and the tricritical point C belongs to this family with $M = 3$.

Notice that the fractional superconformal symmetry is only valid for the two-dimensional wave function. The quantum self-duality is necessary for the fractional superconformal symmetry. Via analyzing the topological anyon sectors of the transfer operators inserted with matrix product operators[31, 32], the continuous topological phase transition along the self-dual line is still driven by the condensation of b anyons[33] (see Supplementary Material). To the best of our knowledge, it is for the first time to find such a tricritical point, and the quantum criticality of this topological phase transition represents a new universality class.

Summary and outlook. - We have fully studied the non-abelian topological phase transitions out of a generic DFib topological state. The key point is the quantum self-duality. Along the self-dual line, three exactly solvable points guide us to map out the global phase diagram. The tensor network representation of the deformed DFib wave function on the square lattice helps us determine the phase boundaries away from the self-dual line. More importantly, a quantum tricritical point represents a new universality class of quantum criticality, where the equal-time correlators are characterized by a coset CFT and the wave function displays an emergent fractional superconformal symmetry. Our method can be extended to study topological phase transitions of other non-abelian topological phases.

A natural question is what relationship between the conformal quantum criticality and the corresponding non-abelian topological phases. Another issue is how the conformal quantum criticality will be changed when the dynamics of the model Hamiltonian for the DFib topological phase is considered. These problems are deserved further considerations. To realize the DFib topological phase experimentally, it is known that parafermions appear in the fractional quantum Hall effect at filling factors $\nu = 1/m$ when two counter-propagating edge states from two adjacent superconducting pairing and spin-orbit induced tunneling[34], and then a two-dimensional array of parafermions can support the Fibonacci anyons[35].

Acknowledgment.- The authors would like to thank Guo-Yi Zhu for his stimulating discussions and acknowledge the support by the National Key Research and Development Program of MOST of China

(2016YFYA0300300).

-
- [1] A. Y. Kitaev, *Annals of Physics* **303**, 2 (2003), ISSN 0003-4916, URL <http://www.sciencedirect.com/science/article/pii/S0003491602000180>.
 - [2] M. H. Freedman, *Communications in Mathematical Physics* **234**, 129 (2003).
 - [3] C. Nayak, S. H. Simon, A. Stern, M. Freedman, and S. Das Sarma, *Rev. Mod. Phys.* **80**, 1083 (2008), URL <https://link.aps.org/doi/10.1103/RevModPhys.80.1083>.
 - [4] M. A. Levin and X.-G. Wen, *Physical Review B* **71** (2005), ISSN 1098-0121, 1550-235X, URL <https://link.aps.org/doi/10.1103/PhysRevB.71.045110>.
 - [5] M. D. Schulz, S. Dusuel, K. P. Schmidt, and J. Vidal, *Phys. Rev. Lett.* **110**, 147203 (2013), URL <https://link.aps.org/doi/10.1103/PhysRevLett.110.147203>.
 - [6] S. Dusuel and J. Vidal, *Phys. Rev. B* **92**, 125150 (2015), URL <https://link.aps.org/doi/10.1103/PhysRevB.92.125150>.
 - [7] M. Mariën, J. Haegeman, P. Fendley, and F. Verstraete, *Phys. Rev. B* **96**, 155127 (2017), URL <https://link.aps.org/doi/10.1103/PhysRevB.96.155127>.
 - [8] A. Feiguin, S. Trebst, A. W. W. Ludwig, M. Troyer, A. Kitaev, Z. Wang, and M. H. Freedman, *Phys. Rev. Lett.* **98**, 160409 (2007), URL <https://link.aps.org/doi/10.1103/PhysRevLett.98.160409>.
 - [9] S. Trebst, E. Ardonne, A. Feiguin, D. A. Huse, A. W. W. Ludwig, and M. Troyer, *Phys. Rev. Lett.* **101**, 050401 (2008), URL <https://link.aps.org/doi/10.1103/PhysRevLett.101.050401>.
 - [10] C. Gils, S. Trebst, A. Kitaev, A. W. W. Ludwig, M. Troyer, and Z. Wang, *Nature Physics* **5**, 834 (2009), ISSN 1745-2473, 1745-2481, URL <http://www.nature.com/articles/nphys1396>.
 - [11] P. Fendley, *Annals of Physics* **323**, 3113 (2008), ISSN 00034916, URL <http://linkinghub.elsevier.com/retrieve/pii/S0003491608000614>.
 - [12] G.-Y. Zhu and G.-M. Zhang, *Phys. Rev. Lett.* **122**, 176401 (2019), URL <https://link.aps.org/doi/10.1103/PhysRevLett.122.176401>.
 - [13] P. Fendley, S. V. Isakov, and M. Troyer, *Physical Review Letters* **110** (2013), ISSN 0031-9007, 1079-7114, URL <https://link.aps.org/doi/10.1103/PhysRevLett.110.260408>.
 - [14] N. Schuch, D. Poilblanc, J. I. Cirac, and D. Pérez-García, *Phys. Rev. Lett.* **111**, 090501 (2013), URL <https://link.aps.org/doi/10.1103/PhysRevLett.111.090501>.
 - [15] J. Haegeman, K. Van Acoleyen, N. Schuch, J. I. Cirac, and F. Verstraete, *Phys. Rev. X* **5**, 011024 (2015), URL <https://link.aps.org/doi/10.1103/PhysRevX.5.011024>.
 - [16] F. Y. Wu, *Reviews of Modern Physics* **54**, 235 (1982), ISSN 0034-6861, URL <https://link.aps.org/doi/10.1103/RevModPhys.54.235>.
 - [17] P. Fendley and J. L. Jacobsen, *Journal of Physics A: Mathematical and Theoretical* **41**, 215001 (2008), ISSN 1751-8113, 1751-8121, URL <http://stacks.iop.org/1751-8121/41/i=21/a=215001?key=crossref.b622c38a08a1779c8dd3baf71daf5bba>.

- [18] V. Dotsenko, J. L. Jacobsen, M.-A. Lewis, and M. Picco, Nuclear Physics B **546** (1999), ISSN 0550-3213, URL <http://www.sciencedirect.com/science/article/pii/S0550321399000978>.
- [19] Z.-C. Gu, M. Levin, B. Swingle, and X.-G. Wen, Physical Review B **79** (2009), ISSN 1098-0121, 1550-235X, URL <https://link.aps.org/doi/10.1103/PhysRevB.79.085118>.
- [20] O. Buerschaper, M. Aguado, and G. Vidal, Physical Review B **79** (2009), ISSN 1098-0121, 1550-235X, URL <https://link.aps.org/doi/10.1103/PhysRevB.79.085119>.
- [21] P. Zanardi, P. Giorda, and M. Cozzini, Phys. Rev. Lett. **99**, 100603 (2007), URL <https://link.aps.org/doi/10.1103/PhysRevLett.99.100603>.
- [22] L. Fidkowski, M. Freedman, C. Nayak, K. Walker, and Z. Wang, Commun. Math. Phys. **287**, 805 (2009), ISSN 1432-0916, URL <https://doi.org/10.1007/s00220-009-0757-9>.
- [23] P. Fendley and E. Fradkin, Phys. Rev. B **72**, 024412 (2005), URL <https://link.aps.org/doi/10.1103/PhysRevB.72.024412>.
- [24] E. Ardonne, P. Fendley, and E. Fradkin, Annals of Physics **310**, 493 (2004), ISSN 00034916, URL <http://linkinghub.elsevier.com/retrieve/pii/S0003491604000247>.
- [25] P. Goodard, A. Kent, and D. Olive, Physics Letters B **152**, 88 (1985), ISSN 03702693, URL <http://linkinghub.elsevier.com/retrieve/pii/0370269385911451>.
- [26] F. Ravanini, Modern Physics Letters A **03**, 397 (1988), ISSN 0217-7323, 1793-6632, URL <http://www.worldscientific.com/doi/abs/10.1142/S0217732388000490>.
- [27] J. Bagger, D. Nemeschansky, and S. Yankielowicz, Phys. Rev. Lett. **60**, 389 (1988), URL <https://link.aps.org/doi/10.1103/PhysRevLett.60.389>.
- [28] D. Bernard and A. Leclair, Physics Letters B **247**, 309 (1990), ISSN 0370-2693, URL <http://www.sciencedirect.com/science/article/pii/037026939090901H>.
- [29] P. C. Argyres, J. M. Grochocinski, and S. H. Henry Tye, Nuclear Physics B **367**, 217 (1991), ISSN 0550-3213, URL <http://www.sciencedirect.com/science/article/pii/0550321391900483>.
- [30] S.-W. Chung, E. Lyman, and S.-H. H. Tye, Int. J. Mod. Phys. A **07**, 3339 (1992), ISSN 0217-751X, URL <https://www.worldscientific.com/doi/abs/10.1142/S0217751X92001484>.
- [31] J. Haegeman, V. Zauner, N. Schuch, and F. Verstraete, NATURE COMMUNICATIONS **6**, 8 (2015), ISSN 2041-1723, URL <http://dx.doi.org/10.1038/ncomms9284>.
- [32] N. Bultinck, M. Mariën, D. J. Williamson, M. B. Şahinoğlu, J. Haegeman, and F. Verstraete, Annals of Physics **378**, 183 (2017), ISSN 0003-4916, URL <http://www.sciencedirect.com/science/article/pii/S0003491617300040>.
- [33] F. A. Bais and J. K. Slingerland, Phys. Rev. B **79**, 045316 (2009), URL <https://link.aps.org/doi/10.1103/PhysRevB.79.045316>.
- [34] D. J. Clarke, J. Alicea, and K. Shtengel, Nature Communications **4**, 1348 (2013).
- [35] R. S. K. Mong, D. J. Clarke, J. Alicea, N. H. Lindner, P. Fendley, C. Nayak, Y. Oreg, A. Stern, E. Berg, K. Shtengel, et al., Phys. Rev. X **4**, 011036 (2014), URL <https://link.aps.org/doi/10.1103/PhysRevX.4.011036>.

SUPPLEMENTAL MATERIAL

Deformed wave function and its norm in the loop basis

In the main text, we have the orthogonal local quantum states $|1\rangle$ and $|\tau\rangle$ on the original lattice and the orthogonal local quantum states $|\hat{1}\rangle$ and $|\hat{\tau}\rangle$ on the dual lattice. They are related by the following transformation

$$\begin{bmatrix} |\hat{1}\rangle \\ |\hat{\tau}\rangle \end{bmatrix} = F \begin{bmatrix} |1\rangle \\ |\tau\rangle \end{bmatrix} = \frac{1}{\phi} \begin{bmatrix} 1 & \sqrt{\phi} \\ \sqrt{\phi} & 1 \end{bmatrix} \begin{bmatrix} |1\rangle \\ |\tau\rangle \end{bmatrix}. \quad (13)$$

It has been proved that the the quantum net wave function takes the same form when rewritten on the dual lattice in the representation of $|\hat{1}\rangle$ and $|\hat{\tau}\rangle$, exhibiting the quantum self-duality. This fact can be understood from the completely packed quantum loop model, from which the Fendley's quantum net originates. The basis for the quantum loop model is given by the completely packed loop configuration \mathcal{L} consisting of two non-orthogonal states $|\tau\rangle$ and $|\hat{\tau}\rangle$, see Fig. 5 (a). Their overlaps are determined as

$$\begin{bmatrix} \langle \tau | \tau \rangle & \langle \tau | \hat{\tau} \rangle \\ \langle \hat{\tau} | \tau \rangle & \langle \hat{\tau} | \hat{\tau} \rangle \end{bmatrix} = \begin{bmatrix} 1 & \lambda \\ \lambda & 1 \end{bmatrix}. \quad (14)$$

According to Eq.(13), the value of λ is determined to $-1/\phi$. So the loop configurations $|\mathcal{L}\rangle$ are non-orthogonal. In the following, we will show that the value of λ can be changed by deforming the wave function. In the non-orthogonal loop basis, the quantum net wave function can be expressed as:

$$|\Psi\rangle = \sum_{\mathcal{L}} \phi^{n_{\mathcal{L}}} |\mathcal{L}\rangle, \quad (15)$$

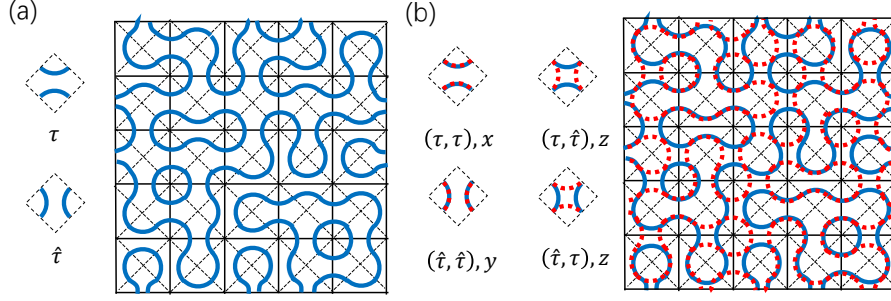


FIG. 5: (a) A typical completely packed loop basis $|\mathcal{L}\rangle$ consists of the local non-orthogonal states $|\tau\rangle$ and $|\hat{\tau}\rangle$, the left and right, up and down sides are connected periodically such that all loops in the configuration are closed. The black full lines are net lattice, the black dash lines are loop lattice, and the blue thick lines are completely packed loop configuration. (b) A typical configuration $(\mathcal{L}, \mathcal{L}')$ of two-coupled completely packed loop model consists of the four local configurations. x , y and z are local Boltzmann weights for these local configurations. The blue full lines stand for the configuration \mathcal{L} form ket, the the red dash lines stand for the configuration \mathcal{L}' form bra.

where $n_{\mathcal{L}}$ is the number of loops in \mathcal{L} and the loop fugacity is ϕ . Under the quantum duality where the $|\tau\rangle$ and $|\hat{\tau}\rangle$ are exchanged with each other, the loop lattice as the medial lattice of the net lattice and dual net lattice is unchanged, so it is obvious that the wave function (15) is invariant. Therefore, when Eq. (15) is expressed in the original lattice on the basis $|1\rangle$ and $|\tau\rangle$ and the dual square lattice on the basis $|\hat{1}\rangle$ and $|\hat{\tau}\rangle$, the wavefunction should have the same form.

Actually the norm of the deformed wave function can be expressed in the non-orthogonal loop basis:

$$\mathcal{Z} = \langle \Psi(h, \hat{h}) | \Psi(h, \hat{h}) \rangle = \sum_{\mathcal{L}, \mathcal{L}'} \phi^{n_{\mathcal{L}} + n_{\mathcal{L}'}} x^{n_{\tau\tau}} y^{n_{\hat{\tau}\hat{\tau}}} z^{n_{\tau\hat{\tau}} + n_{\hat{\tau}\tau}}, \quad (16)$$

where \mathcal{L} and \mathcal{L}' are the loop configurations coming from ket and bra separately and the loop fugacity is the global part of Boltzmann weights. x , y and z are the local Boltzmann weights for four local configurations in Fig. 5 (b), while $n_{i,j}$ with $i, j = \tau, \hat{\tau}$ is the total number of local configurations (i, j) in the global configuration $(\mathcal{L}, \mathcal{L}')$, see Fig.5 (b). The values of x, y and z are determined by the matrix elements of the squared deformation matrix P^2 in non-orthogonal basis:

$$\begin{aligned} x &= \langle \tau | P^2(h, \hat{h}) | \tau \rangle = \left(1 - h + \hat{h}\right)^2 - \frac{4\hat{h}}{\phi^2} (1 - h), \\ y &= \langle \hat{\tau} | P^2(h, \hat{h}) | \hat{\tau} \rangle = \left(1 + h - \hat{h}\right)^2 - \frac{4h}{\phi^2} (1 - \hat{h}), \\ z &= \langle \tau | P^2(h, \hat{h}) | \hat{\tau} \rangle = \langle \hat{\tau} | P^2(h, \hat{h}) | \tau \rangle = -\frac{1}{\phi} \left(1 - h - \hat{h}\right)^2 + \frac{4h\hat{h}}{\phi^2}. \end{aligned} \quad (17)$$

Then the wave function norm can be regarded as the partition function of a two-coupled loop model. On the self-dual line $h = \hat{h}$, we have

$$x = y = 1 - \frac{4h}{\phi^2} (1 - h), \quad z = -\frac{1}{\phi} (1 - 2h)^2 + \frac{4h^2}{\phi^2}, \quad (18)$$

and the partition function (16) is simplified as

$$\mathcal{Z} = \langle \Psi(h, h) | \Psi(h, h) \rangle \propto \sum_{\mathcal{L}, \mathcal{L}'} \phi^{n_{\mathcal{L}} + n_{\mathcal{L}'}} \lambda^{n_{\tau\tau} + n_{\hat{\tau}\tau}}. \quad (19)$$

with

$$\lambda = \frac{z}{x} = \frac{4h^2 - (2h - 1)^2 \phi}{(2h - 1)^2 + \phi}, \quad (20)$$

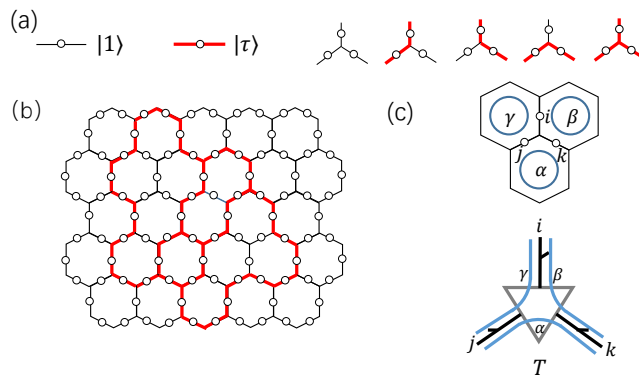


FIG. 6: (a) Two orthogonal quantum states $|1\rangle$ and $|\tau\rangle$ on an edge, and the five local configurations allowed by the branching rule on a vertex of trivalent lattice. The circles represent the physical degrees of freedom. (b) A typical net configuration on a honeycomb lattice, the τ strings formed by $|\tau\rangle$ states are closed and allowed to branch. (c) Up panel: The physical indices i, j, k of the local tensor locate at the edges and auxiliary indices t, s, u live in the plaquette of the lattice. Lower panel: The triplet-line local tensor T_{tsu}^{ijk} on the vertex of the honeycomb lattice for the string-net ground state. The legs of the tensor connected by lines with only one index for simplicity are locked by delta function, and the legs pointed out side of the paper are physical indices.

which is precisely the overlap between two non-orthogonal local states in Eq.(14). This fact can be easily understood from the local configurations $(\tau, \hat{\tau})$ and $(\hat{\tau}, \tau)$ in Fig. 5 (b). So we find that, the effect of tuning the filter strength along the self-dual line $h = \hat{h}$ is equivalent to changing the overlap $\langle \tau | \hat{\tau} \rangle = \langle \hat{\tau} | \tau \rangle$. The wavefunction norm on the self-dual line in Eq. (19) is nothing but the self-dual coupled loop model. The range of parameter on the self-dual line is limited to $h \in [0, \frac{\phi}{2}]$, corresponding to the range of $\lambda \in [-1/\phi, 1]$.

In the loop representation, the decoupled point D on the self-dual line is obviously when $\lambda = 1$ or $h = \frac{\phi}{2}$, and the partition function is $\mathcal{Z} \propto \sum_{\mathcal{L}, \mathcal{L}'} \phi^{n_{\mathcal{L}} + n_{\mathcal{L}'}}$. At this point each loop model is critical. However, the strongly coupled point S is given by $\lambda = 0$ corresponding to $h = \frac{\phi^2}{2} (1 - \sqrt{\phi})$ and $\mathcal{Z} \propto \sum_{\mathcal{L}} \phi^{2n_{\mathcal{L}}}$. This loop model is non-critical because the fugacity $\phi^2 > 2$. In addition to these special points, it is pointed out that there is a new critical point C on the self-dual line. The transfer operator of the self-dual coupled Potts model can be written in terms of a special $SO(4)_3$ Birman-Murakami-Wenzl algebra. By the level-rank duality of the algebra, the position of the new critical point is determined by $\lambda = -\sqrt{2} \sin \frac{\pi}{20}$ corresponding to $h \approx 0.196952$.

Tensor network representation of the Fendley's quantum net

So far the quantum net wave function on a square lattice have not been written in the tensor network representation, because the chromatic polynomial as a non-local topological part of the ground state weight is difficult to deal with. Here we would like to construct a triple-line tensor network state (TNS) for the quantum net on a square lattice.

First of all, we start from the known TNS for the string-net model on a honeycomb lattice. The physical degrees of freedom located at the edges has two orthogonal quantum states labelled by $|1\rangle$ and $|\tau\rangle$, as shown in Fig.6 (a). The branching symbol δ_{ijk} stemming from the non-Abelian fusion rule imposes the branching rule on the vertices. It allows the following five configurations shown in Fig.6 (a), corresponding to the non-zero elements of δ_{ijk} :

$$\delta_{111} = \delta_{1\tau\tau} = \delta_{\tau 1\tau} = \delta_{\tau\tau 1} = \delta_{\tau\tau\tau} = 1. \quad (21)$$

Therefore, in the ground state wavefunction, $|\tau\rangle$ states form a closed trivalent net \mathcal{N} consisting of τ strings, a typical net is displayed in Fig.6 (b).

With the chromatic polynomial, the ground state wavefunction for the Fibonacci string-net can be explicitly expressed as

$$|\Psi_{\text{SN}}\rangle = \sum_{\mathcal{N}} \phi^{3t_{\mathcal{N}}/4} \chi_{\mathcal{N}}(\phi^2) |\mathcal{N}\rangle, \quad (22)$$

where $t_{\mathcal{N}}$ is the number of vertices in the net \mathcal{N} and three τ strings meet together. So $\phi^{3/4}$ can be viewed as the vertex fugacity. The chromatic polynomial is non-local, and it only relates to the topological properties of the net

\mathcal{N} . To represent the non-local wavefunction locally, the auxiliary degrees of freedom have to be introduced, and the wavefunction can be decomposed into a local structure, i.e., the triplet-line tensor network states (TNS):

$$|\Psi_{\text{SN}}\rangle = \sum_{\{ijk\}} \text{tTr} \left[\bigotimes_{\text{vertex}} T_{\alpha\beta\gamma}^{ijk} \right] |\cdots ijk \cdots\rangle, \quad (23)$$

where $T_{\alpha\beta\gamma}^{ijk} = (a_\alpha a_\beta a_\gamma)^{1/6} \sqrt{v_i v_j v_k} G_{\alpha\beta\gamma}^{ijk}$ is the local tensor for the string-net model, and "tTr" denotes the contraction over all virtual indices α, β, γ . G, v and a tensors are uniquely determined by the Fibonacci topological order, and $v_i = \sqrt{d_i}$, $a_i = d_i / (\sum_i d_i^2)$ with $d_1 = 1$, $d_\tau = \phi$ as the quantum dimensions. Moreover, $G_{\alpha\beta\gamma}^{ijk} = \delta_{ij\gamma} \delta_{\alpha\beta\gamma} \delta_{i\beta k} \delta_{j\alpha k} \frac{F_{\alpha\beta\gamma}^{ijk}}{v_k v_\gamma}$, and the F -symbol is given by:

$$F = \begin{pmatrix} F_{\tau\tau 1}^{\tau\tau 1} & F_{\tau\tau\tau}^{\tau\tau 1} \\ F_{\tau\tau 1}^{\tau\tau\tau} & F_{\tau\tau\tau}^{\tau\tau\tau} \end{pmatrix} = \frac{1}{\phi} \begin{pmatrix} 1 & \sqrt{\phi} \\ \sqrt{\phi} & -1 \end{pmatrix}. \quad (24)$$

The graphical representation of the T tensor is shown in Fig.6(c).

In the main text, the wavefunction of quantum net is defined by

$$|\Psi\rangle = \sum_{\mathcal{N}} \phi^{-L_{\mathcal{N}}/2} \chi_{\mathcal{N}}(\phi^2) |\mathcal{N}\rangle, \quad (25)$$

where $L_{\mathcal{N}}$ is total length of τ string in net \mathcal{N} . Note that the difference between string-net wavefunctions in Eq. (22) and quantum net in Eq. (25) is the local parts of the ground state weights and the types of the lattice. The local parts (string tension and vertex fugacity) are very easy to deal with, so the key point is to represent the chromatic polynomials for nets on the square lattice in terms of tensor networks. From Eqs. (22) and (23), we notice the correspondence between the chromatic polynomials for nets on the honeycomb lattice and the tensor networks is

$$\chi_{\mathcal{N}_{\text{hyc}}}(\phi^2) \Leftrightarrow \text{tTr} \left(\bigotimes_{\text{vertex}} \tilde{T}_{\alpha\beta\gamma}^{ijk} \right), \quad (26)$$

where "hyc" stands for the honeycomb lattice and $\tilde{T}_{tsu}^{ijk} = \phi^{-\frac{3}{4} \delta_{i,j} \delta_{j,k} \delta_{k,\tau}} T_{tsu}^{ijk}$. Since the ground states are degenerate, two above expressions might not be equal.

Thanks to the equations among the chromatic polynomials shown in Fig. 7 (a), we can obtain the relation between $\chi_{\mathcal{N}_{\text{hyc}}}(Q)$ and $\chi_{\mathcal{N}_{\text{sq}}}(Q)$. More specifically, we can transform the square lattice into a honeycomb lattice by splitting all the sites and adding new edges, as shown in Fig. 7. There exist two different ways of splitting a single site, but the results are equivalent to each other. A new created edge can be either occupied by τ string or unoccupied. For a net on the square lattice, it might include the bivalent, trivalent and tetra-valent vertices. After the lattice transformation, there is no ambiguity for both bivalent and trivalent vertices, because the chromatic polynomials for open nets are zero. For a net with one tetra-valent vertex, its chromatic polynomial becomes a sum of two chromatic polynomials on the honeycomb lattice, as shown in Fig. 7 (b). If a net on the square lattice has n tetra-valent vertices, its chromatic polynomial is a sum over $2n$ chromatic polynomials on the honeycomb lattice.

Conversely, for the wave function with the weight $\chi_{\mathcal{N}_{\text{hyc}}}(\phi^2)$ on the honeycomb lattice, summing over physical degrees of freedom on the new edges (NE) of the honeycomb lattice yields the wave function weighted by $\chi_{\mathcal{N}_{\text{sq}}}(\phi^2)$ on the square lattice:

$$\sum_{\mathcal{N}_{\text{sq}}} \chi_{\mathcal{N}_{\text{sq}}}(\phi^2) |\mathcal{N}_{\text{sq}}\rangle = \left[\bigotimes_{\text{NE}} \sum_{i=1,\tau} \langle i| \right] \left[\sum_{\mathcal{N}_{\text{hyc}}} \chi_{\mathcal{N}_{\text{hyc}}}(\phi^2) |\mathcal{N}_{\text{hyc}}\rangle \right]. \quad (27)$$

This is the relation between $\chi_{\mathcal{N}_{\text{hyc}}}(Q)$ and $\chi_{\mathcal{N}_{\text{sq}}}(Q)$, which only involves some local operations. So the connection between the local tensors for a string-net and local tensors for a quantum net is clear. Although the TNS representation and chromatic polynomial representation of the ground state might not be equal, the two expressions can not be distinguished locally. The TNSs for a string-net on the honeycomb lattice and the corresponding quantum net on the square lattice obey the same relation:

$$\sum_{\{ijkl\cdots\}} \text{tTr} \left(\bigotimes_{\text{vertex}} T_{sq} \right) |ijkl\cdots\rangle = \left[\bigotimes_{\text{ne}} \sum_{i=1}^{\tau} \langle i| \right] \left[\sum_{\{ijk\cdots\}} \text{tTr} \left(\bigotimes_{\text{vertex}} \tilde{T} \right) |\cdots ijk \cdots\rangle \right]. \quad (28)$$

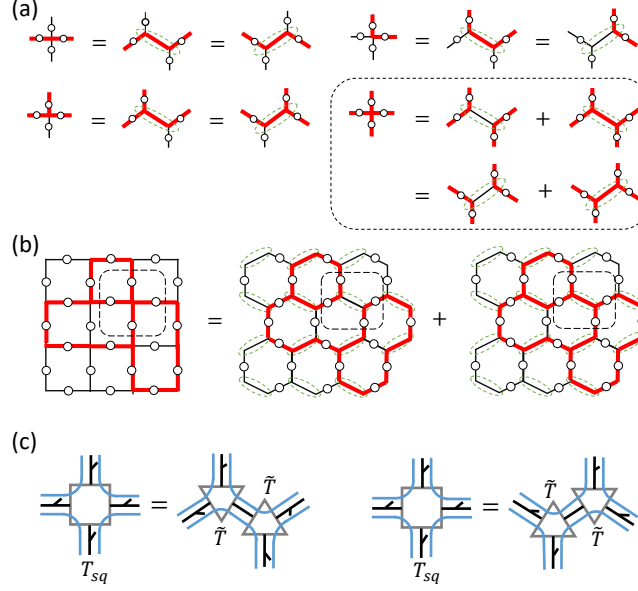


FIG. 7: (a) The square lattice can be transformed to a honeycomb lattice by splitting a lattice site into two sites and adding new edges (in the green ovals), notice that on the new edges there is no physical degree of freedom. There are two equivalent ways of doing this. The single τ string on the vertex of square lattice is transformed into a single τ string on the vertices of the honeycomb lattice, displayed by the first three equations. The fourth equation in the box shows that the tetra-valent vertex on a square lattice where two τ strings meet can be reduced to the sum of two graphs on the honeycomb lattice. (b) The chromatic polynomial for a square lattice net with a tetra-valent vertex (in the box with dash line) is equal to the sum of two chromatic polynomials for the honeycomb lattice nets. (c) Contracting two tensors \tilde{T} along one bond direction of the string-net TNS, we obtain the tensor T_{sq} for Fendley's wavefunction. Because there are two equivalent ways of transforming the vertex of a square lattice into two vertices of the honeycomb lattice, there are two kinds of T_{sq} tensors. Notice that the physical index between two \tilde{T} tensors belonging to the new edges is summed.

In this TNS, the sum over physical degrees of freedom on new edges is equivalent to that there is no physical degrees on these new edges. Hence, the local tensor T_{sq} for a square lattice quantum net is given by combining two tensors \tilde{T} along one bond direction of the honeycomb lattice, as displayed in Fig. 7 (c). Taking the string tension into account, the TNS for the quantum net on the square lattice is thus given by

$$|\Psi\rangle = \sum_{\{ijkl\dots\}} \text{tTr} \left(\bigotimes_{\text{vertex}} \phi^{-\frac{i+j+k+l}{4}} T_{sq} \right) |ijkl\dots\rangle, \quad (29)$$

where the string tension on each tensor reduces to $\phi^{1/4}$.

Transfer operator and matrix product operator

In order to detect the mechanism of the quantum phase transition, we analysis the fate of anyons with matrix product operator (MPO). The MPO acts on virtual indices of the tensor networks, satisfying the pulling through condition, so the invisible MPO can be moved freely. Although our TNS for the quantum net is different from the string-net TNS, their MPOs are the same. The reason is that the local tensor T_{sq} comes from local tensor T of the string-net, we only do some local operations on the physical degrees of freedom of the tensor, while the auxiliary degrees of freedom that MPO acts on remain unchanged. This is also an evidence that the quantum net on the square lattice and the string-net have the same topological order, because the MPO algebra is a necessary condition for topologically ordered TNS.

The local tensor of MPO is also determined by G and v tensors. There are two local tensors

$$B_{1,(jl),(im)}^{(jki),(lkm)} = G_{lm1}^{ijk} \sqrt{v_i v_j v_l v_m}, \quad B_{\tau,(jl),(im)}^{(jki),(lkm)} = G_{lm\tau}^{ijk} \sqrt{v_i v_j v_l v_m}, \quad (30)$$

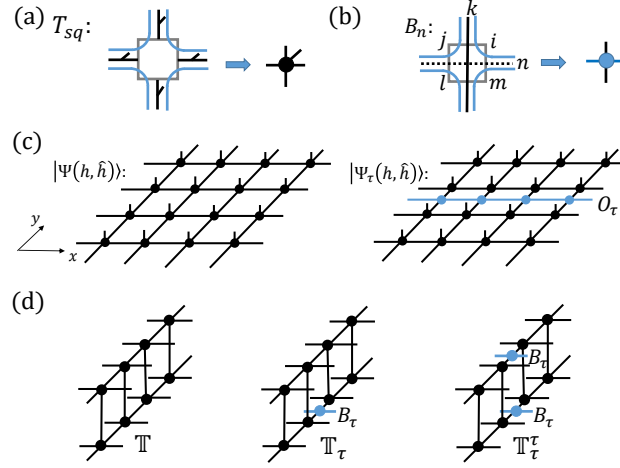


FIG. 8: (a) A simplified graphic representation for the local tensor T_{sq} of the deformed wavefunction $|\Psi(h, \hat{h})\rangle$. (b) The local tensor B_n generating the MPO O_n , where $n = 1, \tau$, and its simplified graphic representation. (c) The tensor networks for wavefunction $|\Psi(h, \hat{h})\rangle$ and $|\Psi_\tau(h, \hat{h})\rangle$ with MPO O_τ (blue line) insertion in x direction. (d) Three inequivalent transfer operators: \mathbb{T} without MPO tensor insertion; \mathbb{T}_τ with MPO tensor B_τ insertion in ket layer and \mathbb{T}_τ^τ with MPO tensor B_τ insertion in both layers.

where the superscripts are the physical indices and the subscribes are virtual indices, as displayed in the right panel of Fig. 8 (a). The MPOs generated by B_1 and B_τ are given by

$$\begin{aligned}
 O_1 &= \sum_{\{(jki), (lkm)\}} \text{tr} \left(\prod_l B_1^{(j_1 k_1 i_1), (l_1 k_1 m_1)} \right) | \{jki\} \rangle \langle \{lkm\} |, \\
 O_\tau &= \sum_{\{(jki), (lkm)\}} \text{tr} \left(\prod_l B_\tau^{(j_1 k_1 i_1), (l_1 k_1 m_1)} \right) | \{jki\} \rangle \langle \{lkm\} |.
 \end{aligned} \tag{31}$$

O_1 is trivial in the sense that it is equivalent to an identity operator, while O_τ is non-trivial, because it has two eigenvalues ϕ and $-\phi^{-1}$. Both O_1 and O_τ satisfy the Fibonacci fusion rule. Notice that these two MPOs are unchanged for different values of h and \hat{h} . To investigate the mechanism of the phase transition, we need to systematically classify the topological sectors of the tensor networks with MPOs.

On a torus, the ground state is degenerate. The other wavefunction denoted by $|\Psi_\tau(h, \hat{h})\rangle$ can be obtained by inserting MPO O_τ into the tensor network, as shown in Fig. 8 (b). The corresponding topological order can be identified from the transfer operator \mathbb{T} of the wavefunction norm

$$\langle \Psi(h, \hat{h}) | \Psi(h, \hat{h}) \rangle = \text{Tr} (\mathbb{T}^{L_x}), \tag{32}$$

where L_x is the length of the lattice in the x -direction and the circumference of the transfer operator \mathbb{T} is denoted by L_y . Since the wavefunction norm is regarded as two coupled ϕ^2 Potts models, the effective dimension of the transfer operator \mathbb{T} is thus given by $\phi^{4L_y} \times \phi^{4L_y}$ for a large L_y . The wavefunction norm thus has the two layers, one is the bra layer and the other is the ket layer. Inserting the MPO O_τ in either bra layer or ket layer, or both layers, results in the norms

$$\begin{aligned}
 \langle \Psi(h, \hat{h}) | \Psi_\tau(h, \hat{h}) \rangle &= \text{Tr} [(\mathbb{T}_\tau)^{L_x}], \\
 \langle \Psi_\tau(h, \hat{h}) | \Psi_\tau(h, \hat{h}) \rangle &= \text{Tr} [(\mathbb{T}_\tau^\tau)^{L_x}].
 \end{aligned} \tag{33}$$

So there are three inequivalent transfer operators \mathbb{T} , \mathbb{T}_τ^τ , and \mathbb{T}_τ or \mathbb{T}^τ , as shown in Fig. 8 (d), where the subscribe (superscribe) stands for the MPO tensor B_τ insertion in the ket (bra) layers.

The anyon sectors of the transfer operators can be classified for the bra and ket layers individually, and they are denoted by $(\alpha|\beta)$, where $\alpha, \beta = 1, \tau, \bar{\tau}, b$ are anyon sectors of the bra and ket, separately. There are in total 16 sectors, in which the topological sectors $(b|b)$, $(\tau|\tau)$ and $(\bar{\tau}|\bar{\tau})$ of the transfer operator measuring the confinement of b , τ and $\bar{\tau}$

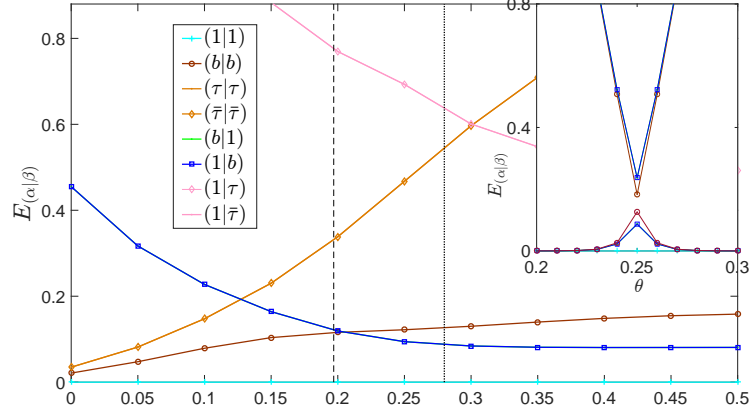


FIG. 9: The values of $E_{(\alpha|\beta)}$ for each anyon sectors $(\alpha|\beta)$ along the self-dual line, obtained from the transfer operator with circumference $L_y = 6$. Inset: The spectrum of transfer operator \mathbb{T} with circumference $L_y = 6$ along the ϕ^4 -state Potts lines. The horizontal axis is labelled by angle of polar coordinate so that the spectrum is symmetric about the self-dual point ($\theta = 0.25\pi$).

anyons and sectors $(1|b)$, $(1|\tau)$ and $(1|\bar{\tau})$ measuring the condensation of b , τ and $\bar{\tau}$ anyons. The dominant eigenvalues of these sectors determine the property of anyons in the thermodynamic limit.

Next, we illustrate how to find dominant eigenvalues and the properties of anyons. By analysis the central idempotent, the layer of a transfer operator without MPO tensor B_τ insertion contains the anyon sectors 1 and b , while the layer with MPO tensor B_τ insertion contains the anyon sector b , τ and $\bar{\tau}$. Therefore, the transfer operator \mathbb{T} includes three anyon sectors:

$$(1|1); (1|b) \ \& \ (b|1); (b|b). \quad (34)$$

\mathbb{T}_τ^τ has the following anyon sectors:

$$(b|b); (b|\tau) \ \& \ (b|\bar{\tau}) \ \& \ (\tau|b) \ \& \ (\bar{\tau}|b); \\ (\tau|\bar{\tau}) \ \& \ (\bar{\tau}|\tau), (\tau|\tau) \ \& \ (\bar{\tau}|\bar{\tau}). \quad (35)$$

And \mathbb{T}_τ contains sectors:

$$(1|b), (1|\tau) \ \& \ (1|\bar{\tau}), (b|\tau) \ \& \ (b|\bar{\tau}), (b|b). \quad (36)$$

Because of the exchanging τ and $\bar{\tau}$ under the time reversal symmetry or the symmetry between bra and ket, some sectors are always exactly degenerate, and they are denoted by the symbol “&”. Moreover, \mathbb{T} commutes with $O_\tau \otimes O_\tau$, the eigenstates of \mathbb{T} are also eigenstates of $O_\tau \otimes O_\tau$ with eigenvalue $\phi^2, -1, -1, 1/\phi^2$ for sectors $(1|1)$, $(1|b) \ \& \ (b|1)$, $(b|b)$, separately. According to the degeneracy of a given level and the associated transfer operator, we can determine the sectors to which the level belongs.

With the dominant eigenvalues of anyon sectors we concern, we can analysis the mechanism for quantum phase transition. For convenience, a quantity is defined $E_{(\alpha|\beta)} = -\log(\frac{e_{(\alpha|\beta)}}{e_{(1|1)}})$, where $e_{(\alpha|\beta)}$ is the dominant eigenvalue of the transfer operator in the sector $(\alpha|\beta)$. So $E_{(1|\beta)}$ measures the condensation of β anyon. As the circumference of the transfer operator $L_y \rightarrow \infty$, the anyons β are condensed if $E_{(1|\beta)} \rightarrow 0$ exponentially with L_y . On the other hand, $E_{(\alpha|1)}$ measures the confinement of α anyons. As the circumference of the transfer operator $L_y \rightarrow \infty$, the anyons are confined if $E_{(\alpha|1)} > 0$.

From the viewpoint of anyon condensation, the only possibility of the Fibonacci topological phase transition is the condensation of b anyons with the confinement of τ and $\bar{\tau}$ anyons. We are curious about whether the phase transition along the self-dual line is beyond the anyon condensation. In analysis below, we make a reasonable assumption that in the gapped phases the splitting between degenerate eigenvalues $E_{(\alpha|\beta)}$ below the gap of the transfer operator spectrum is exponential small with the system size.

In the left panel of Fig. 9 we show the variation of $E_{(\alpha|\beta)}$ along the self-dual line. It implies that in the topological phase, $E_{(b|b)}$, $E_{(\tau|\tau)}$ and $E_{(\bar{\tau}|\bar{\tau})}$ approach to zero exponentially, so b , τ and $\bar{\tau}$ anyons are not confined. $E_{(1|b)}$, $E_{(1|\tau)}$ and $E_{(1|\bar{\tau})}$ are above the spectrum gap, so that the b , τ and $\bar{\tau}$ are not condensed. On the first-order phase transition line, there is a much longer correlation length and an approximate conformal invariance. Thus it is not easy to distinguish

TABLE II: Scaling dimensions of the primary fields in the 2nd unitary minimal model with the central charge $c = \frac{7}{10}$. The third column is the results extracted from the transfer operator with circumference $L_y = 12$ numerically, and the spectrum of the transfer operator is rescaled such that the scaling dimensions of the first descendents of identity field are 1. The second column is the Neveu-Schwarz (NS) sector and Ramond (R) sector of the theory.

scaling dimension	sector	Numerical result	Error
0	NS	0	0
3/40	R	0.07139148	0.0036
1/5	NS	0.18874674	0.0113
7/8	R	0.84037430	0.0346

the gap and the degeneracy below the gap on the first-order transition line with such a small system size. To resolve the problem, we plot the ϕ^4 -state Potts line in the insert of Fig. 9, where $\theta = 0.25\pi$ corresponds to $h \simeq 0.279$ on the self-dual line. From the inset, the dominant eigenvalues $E_{(1|b)}$, $E_{(b|1)}$ and $E_{(b|b)}$ and the subdominant eigenvalues for the three topological sectors are degenerate with $E_{(1|1)}$ in the thermodynamical limit due to the level crossings at the first order transition line. The splitting between them is exponentially small for a finite size system. We can conclude that $E_{(1|b)} \rightarrow 0$ exponentially with $L_y \rightarrow \infty$ because it is below the gap. So along the self-dual line, it still exhibits the b anyon condensation. In addition, $E_{(b|b)} \rightarrow 0$ exponentially with $L_y \rightarrow \infty$, indicating that b anyons are not confined. Meanwhile, $E_{(\tau|\tau)}, E_{(\bar{\tau}|\bar{\tau})} > 0$ imply the τ and $\bar{\tau}$ anyons are confined.

Finite-size spectrum of conformal field theory

In the view point of statistical model, the point D in the phase diagram corresponds to the critical point of two decoupled ϕ^2 -state Potts models, and we can still calculate the transfer operator spectrum at the point D to check the validity of our TNS. The single ϕ^2 -state Potts model at the critical point is described by the second unitary minimal conformal field theory (CFT) with the central charge $c = 7/10$. This CFT is also the first unitary minimal superconformal model, and it is the only theory with both Virasoro and super-Virasoro minimal. The scaling dimensions of primary fields of the CFT are listed in Tab. II, and our numerical results match with such a prediction. The total central charge of two decoupled models is $7/5$.

At the critical point A on the \hat{h} axis, the critical theory is described by the seventh unitary minimal CFT with the central charge $c = 14/15$, which belongs to another family of CFT. The corresponding central charge c and scaling dimensions $\mathfrak{h}_{r,s}$ of primary fields are given by

$$c = 1 - \frac{6}{m(m+1)}, \quad m \geq 3,$$

$$\mathfrak{h}_{r,s} = \frac{[(m+1)r - ms]^2}{4m(m+1)}, \quad 1 \leq r < m, \quad 1 \leq s \leq r. \quad (37)$$

Our case corresponds to $m = 9$ and the scaling dimensions of the primary fields are listed in Tab. III. Notice that only primary fields with $r = \text{odd}$ in the minimal model appear in our microscopic model. The critical theory of the point B has the same CFT due to the quantum duality.

Along the h axis, the effective dimension of the transfer operator \mathbb{T} can be reduced from $\phi^{4L_y} \times \phi^{4L_y}$ to $(\phi+2)^{L_y} \times (\phi+2)^{L_y}$, and the number of degrees of freedom coincides with the $(\phi+2)$ -state Potts model. We also calculate the transfer operator spectrum of the string-net model, which can be exactly mapped to the $(\phi+2)$ -state Potts model. From the comparison between the transfer operator spectra of the string-net and quantum net, we suspect that the larger errors for the scaling dimensions of some primary fields seen Tab. III may be caused by the fact that the quantum net model does not exactly correspond to the $(\phi+2)$ -Potts model.

Finally, the tri-critical point C in the phase diagram is characterized by the coset CFT of $\frac{SU(2)_3 \times SU(2)_3}{SU(2)_6}$, which belongs to the series of models with fractional superconformal symmetry. The central charge c and conformal dimensions

TABLE III: Scaling dimensions $\mathfrak{h}_{r,s} + \bar{\mathfrak{h}}_{r,s}$ of the primary fields in the seventh unitary minimal model with the central charge $c = \frac{14}{15}$. The third and fourth columns are the scaling dimensions numerically extracted from the transfer operator of the quantum net with circumference $L_y = 10$ and their errors. The fifth and sixth columns are the scaling dimensions numerically extracted from the transfer operator of the string-net with a circumference $L_y = 10$ and their errors. The spectrum of transfer operator is rescaled such that the scaling dimension of the first descendent of $\mathfrak{h}_{r,s} + \bar{\mathfrak{h}}_{r,s} = 0$ is 1. The absolute errors of data with a star are larger than 10% compared with exact scaling dimension.

(r, s)	$\mathfrak{h}_{r,s} + \bar{\mathfrak{h}}_{r,s}$	Quantum net	Error	String-net	Error
(1, 1)	0	0	0	0	0
(3, 3)	2/45	0.04973837	0.0053	0.04369855	0.0007
(5, 5)	2/15	0.14089491	0.0076	0.12985540	0.0035
(5, 5)	2/15	0.14089491	0.0076	0.12985540	0.0035
(7, 7)	4/15	0.23521085	0.0315	0.25426793	0.0124
(2, 1)	2/3	0.94338622*	0.2767	0.72615165	0.0595
(4, 3)	14/15	0.94457473	0.0112	0.93859015	0.0053
(6, 5)	56/45	0.95672807*	0.2877	1.19624200	0.0482
(6, 5)	56/45	0.95672807*	0.2877	1.19624200	0.0482
(8, 7)	8/5	0.98182889*	0.6182	1.44124861	0.1588

$\mathfrak{h}_{p,q}$ of primary fields for the $\frac{SU(2)_k \times SU(2)_m}{SU(2)_{k+m}}$ coset CFT are given by

$$c = 1 - \frac{6m}{(k+2)(k+m+2)} + \frac{2(m-1)}{m+2},$$

$$\mathfrak{h}_{p,q} = \frac{[(k+m+2)p - (k+2)q]^2 - k^2}{4m(k+2)(k+m+2)} + \frac{t(m-t)}{2m(m+2)}, \quad (38)$$

where $t = (p - q) \bmod m$, $1 \leq p \leq k + 1$ and $1 \leq q \leq k + 1 + m$. The tricritical point C corresponds to $m = k = 3$, and the corresponding finite-size spectrum has been included in the main text.